Review

Check for updates

An overview of bearing voltages and currents in rail transportation traction motors

Yao LI[1], Lin QIU[1✉], Yongjian ZHI[2], Zifan GAO[2], Jien MA[1], Jian ZHANG[1], Youtong FANG[1]

[1]*College of Electrical Engineering, Zhejiang University, Hangzhou 310027, China*
[2]*CRRC Zhuzhou Institute Co. Ltd., Zhuzhou 412001, China*

Abstract: In modern rail transportation, inverter drive systems have been extensively used due to their excellent speed control capabilities. However, in recent years, premature failure problems caused by bearing voltage and current phenomena have been frequently reported in electric motors, with electrical bearing failures making up a considerable percentage. The purpose of this review is to provide a comprehensive overview of facets relating to the electrical erosion of bearings in an electrical environment represented by railway vehicles. First, the origins of the phenomenon as well as typical bearing electrical failure modes are discussed. Next, we introduce the distinctive features of the electrical environment of railway traction motor bearings, including output voltages with high common-mode components and systems with complex grounding configurations. Then, we classify the fundamental mechanisms for generating bearing voltages/currents into four groups, and present their modeling processes, including equivalent circuit establishment and parameter determination methods. Furthermore, we summarize the strategies frequently used to protect bearings, and describe a typical solution to suppress electrical bearing failures in railway vehicles. Finally, we present a case example to illustrate a research procedure for systematic investigation of inverter-induced bearing currents in rail transportation.

Key words: Rail transportation; Bearing current; Common-mode voltage; Bearing electrical erosion; Grounding configuration

1 Introduction

In the context of electrical drives, nearly half of motor failures are due to rolling element bearing failures, which are the primary cause of downtime (Bonnett and Yung, 2006; Zhang et al., 2011). Among the causes of the bearing faults, bearing voltages and associated bearing currents are well known to accelerate bearing degradation. According to their mode of generation, bearing voltages are divided into two categories: magnetic flux asymmetry and inverter-induced voltage effects.

The existence of alternating shaft voltages in line-operated electrical machines was first reported early in the 20th century (Punga and Hess, 1907; Fleishmann, 1910). Investigators found that such voltages may cause a circulating current across the bearings, which reduces their life. Alger and Samson (1924) considered unbalanced magnetic fields to be the cause of this kind of bearing current. For a four-pole electric machine, the flux of each pole after crossing the air gap can be categorized into a clockwise flux and a counterclockwise flux through the yoke (Fig. 1). Due to manufacturing details such as axial cooling holes in the stator lamination joints between stator segments, regions A and C have a much higher reluctance than regions B and D. Thus, pole 1 sends most of its flux through D to pole 4 in a clockwise direction, leading to a parasitic alternating-current (AC) magnetic flux $\phi_{parasitic}$ surrounding the motor shaft, which further produces the shaft voltage during the rotational process of cutting the magnetic induction line. In the decades that followed, numerous researchers conducted thorough studies on classical bearing currents, and the problem was fixed with advances in motor manufacturing specifications and the implementation of bearing protection strategies (Alger and Samson, 1924; Boyd and Kaufman, 1958; Ammann et al., 1988;

✉ Lin QIU, qiu_lin@zju.edu.cn

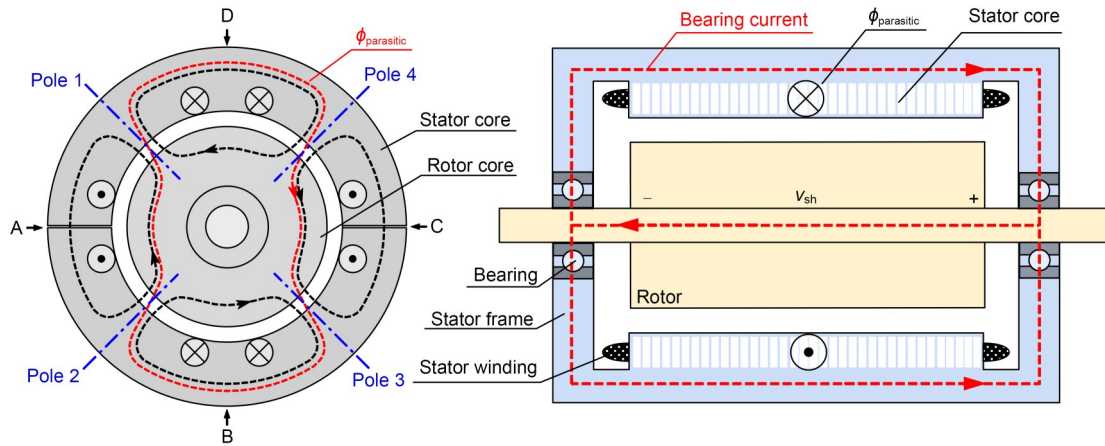Lin QIU, https://orcid.org/0000-0003-1236-2191

Fig. 1 Bearing currents due to magnetic asymmetries. v_{sh} is the shaft voltage

Buckley et al., 1988; Costello, 1993; Raymond, 1999). For industry applications, IEEE112 gives guidelines for monitoring shaft voltages and defines thresholds for shaft or bearing voltages of machines under traditional operation (IEEE, 1997).

In recent decades, pulse width modulation (PWM) inverters with high-performance semiconductor switching devices have been frequently used in modern electric vehicles to achieve variable speed control. However, electric motors operated by PWM inverters are subjected to high-frequency (HF) bearing currents that were not previously a problem. The phenomena of HF bearing currents were first explained and modeled (Chen SM et al., 1996; Chen ST et al., 1996; Chen and Lipo, 1998). The non-zero common mode (CM) voltage generated by the PWM inverters is regarded as the source, and the capacitive coupling paths consist of the stator winding-to-frame capacitance C_{wf}, rotor-to-frame capacitance C_{rf}, stator winding-to-rotor capacitance C_{wr}, and bearings C_{b}. Four types of HF bearing currents can be distinguished: dv/dt bearing currents (where v is the voltage and t is the time), electric discharge machining (EDM) bearing currents, circulating bearing currents, and rotor ground bearing currents (Fig. 2). Due to the presence of coupling capacitances, a voltage drop v_{b} across the bearing which mirrors the CM voltage is generated. With an intact lubricating film, dv/dt bearing currents flow through the path of the "stator winding–rotor–bearing–stator frame." When v_{b} exceeds the breakdown voltage of the lubrication, the C_{rf} discharges over the shorted bearing, leading to EDM bearing currents. The HF ground current caused by the C_{wf} produces a flux encircling
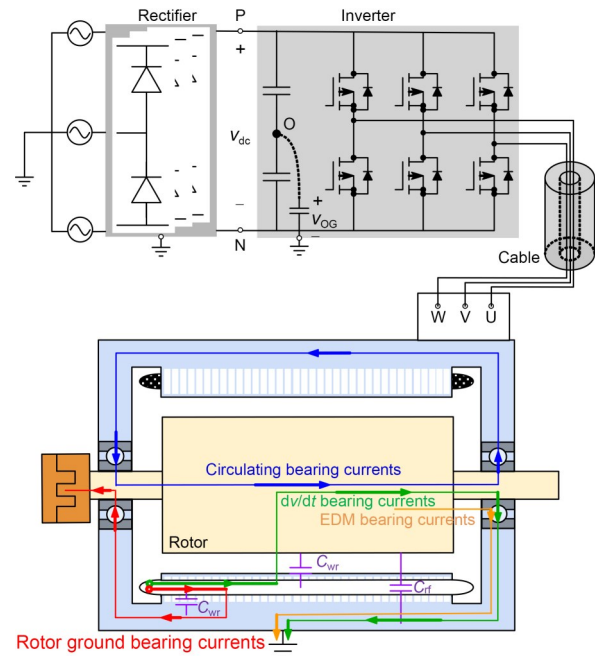

Fig. 2 Bearing currents due to inverter operation. v_{dc} is the direct current (DC)-link voltage; v_{OG} is the voltage of virtual neutral point O to ground. P and N are the positive and negative DC rails, respectively; U, V, and W represent the three inverter phases

the shaft, creating circulating bearing currents along the loop of the "stator frame–non drive end–shaft–drive end." Rotor ground bearing currents occur when the rotor is connected to the ground with a lower impedance path than the stator frame. In this case, part of the overall ground current flows through the "stator winding–stator frame–bearing–rotor–ground." A zero sequence equivalent circuit model for electrical analysis of EDM currents has been proposed and the related

model parameter formulas derived (Busse et al., 1997a, 1997b, 1997c, 1997d, 1997e). With the calculated bearing current density, the electrical bearing life can be estimated (Busse et al., 1997a, 1997c). Muetze (2004) published a series of papers, including: a systematic summary of bearing currents generation theory, improved approaches for the calculation of related parameters (Muetze and Binder, 2007b), analytical calculation and measurement for EDM currents (Muetze, 2004), modeling and calculation of circulating bearing currents (Muetze and Binder, 2007a), guidelines for bearing currents assessment (Muetze and Binder, 2007c), and mitigation technique selection (Muetze and Binder, 2006). Industrial measurement techniques for HF bearing voltages and currents are now provided by various bearing companies. A simple but intrusive way to measure the bearing voltages involves the use of shaft brushes (AEGIS, 2007). SKF (2014) used an electrical discharge detector pen to count the number of discharges to estimate the extent and severity of the bearing defect. In addition, Rogowski coils are widely used to monitor ground currents associated with high dv/dt (ABB, 2021). A patented solution for bearing current protection was provided by AEGIS. This solution consists of a conductive ring mounted on the shaft, providing a low-impedance path to the ground for bearing currents, and is now used widely (Muetze and Oh, 2008a, 2008b). Recently, diagnostic methods based on artificial intelligence (AI) have attracted much attention (Cheng et al., 2020; Zhang et al., 2020; Shamsirband and Khansari, 2021). SKF (2019, 2022) used AI visual to differentiate electrical current damage from abrasive wear. Other measurement and mitigation techniques can be found in IEC60034-25 (IEC, 2014).

The problem of electric currents passing through rolling bearings and causing damage in the contact area of rollers and inner/outer ring raceways is well-known, leading to a new kind of failure mode. The electric-related damage can be divided into five types: pitting, frosting, fluting, white etching cracks, and grease degradation (Boyanton and Hodges, 2002; Sunahara et al., 2011; Tischmacher and Gattermann, 2012a, 2012b; AEGIS, 2018; Plazenet and Boileau, 2021). Once the bearing voltage reaches a level sufficient to overcome the dielectric properties of the bearing grease, they arc through the motor's bearings, leaving small craters on the metallic surface, formed by the local melting of the metal due to the arc current. These pits have an average diameter of about 0.5 μm and can be seen using scanning electron microscopy (Fig. 3a) (AEGIS, 2018). The frosting consists of
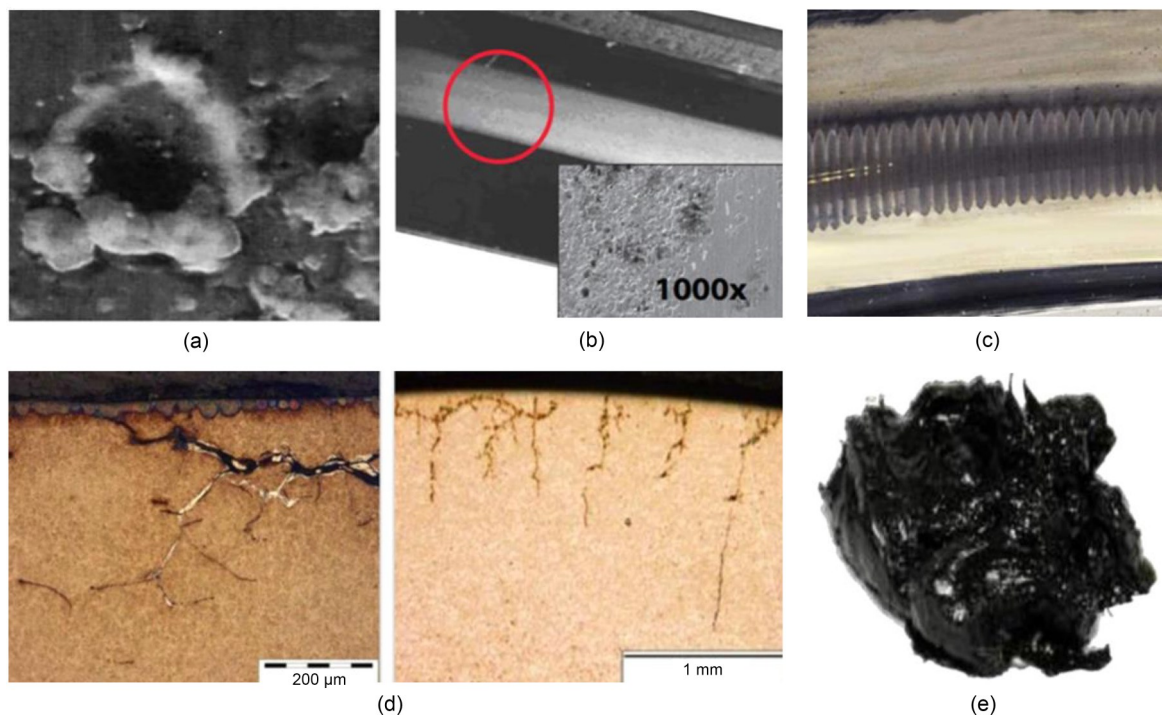

Fig. 3 Electrical bearing failure modes: (a) pitting; (b) frosting; (c) fluting; (d) white etching cracks; (e) grease degradation

countless pits caused by frequent discharges, and appears as a grey discolored line around the bearing race. Fig. 3b shows an example of the frosting as seen under a microscope (AEGIS, 2018). Fluting is the most common pattern seen on visual inspection of the bearings, and is characterized by rolling axis paralleled and equally spaced flutes. The washboard-like ridges such as those shown in Fig. 3c (AEGIS, 2018) cause vibration and noise and indicate a catastrophic bearing failure. Meanwhile, bearing currents have been regarded as one of the factors inducing white etching cracks. A rolling contact fatigue mode will develop into irreversible brittle flaking, spalling, or radial cracking of bearing components, and is characterized by a wide subsurface network of cracks typically from 0.1 to 1.0 μm in width (Fig. 3d) (Plazenet and Boileau, 2021). In addition, the energy released by bearing current discharge events may cause grease degradation, which is a self-amplifying process (Tischmacher and Gattermann, 2012b). With a degraded lubrication film, the vibration level and frequencies increase (Tischmacher and Gattermann, 2012a), which further affects film thickness and the electrical field strength, increasing the number of voltage breakdowns in a certain period. As a result, corrugated patterns are formed, which in turn increase the vibration levels. Fig. 3e depicts the burnt grease (AEGIS, 2018).

Over the years, electrical bearing failures are more likely to occur in rolling mills because of their poor working conditions, including heavy impact, excessive radial and axial loads, and high temperature. However, with the development of rail transportation, bearing failures in railway traction motors have been widely reported due to long operation times and complex and harsh environments. Fig. 4 shows inverter-induced bearing damage in railway vehicles. Since the assembly and disassembly of bearings are complicated, the bearing failures in a running train are difficult to detect in the early stages using traditional fault diagnostic techniques. This not only adds to the cost of bearing replacement, but also poses potential threats to the safe and stable operation of the traction system. The consequences of bearing damage range from train delay and suspension to train brake failure and accidents. Unlike in other AC motor applications, inverter-induced electrical erosion in rail transportation has the following special features: (1) It has a high CM component in inverter output voltages with high dv/dt.

Considering the high voltage and large current in practical onboard traction converters, the switching frequency is limited to several hundred Hz to reduce switching loss, which is close to the output frequency of the converter in the high-speed region. Thus, synchronized modulation strategies and a six-step operation are adopted (Zhao et al., 2020), which generate high dv/dt stepwise CM voltage between the motor neutral and its stator frame. (2) It has a complicated grounding configuration. In ideal cases, the stator frame is grounded to earth with a low-impedance cable, and the rotor is not grounded. However, in railway vehicles, the impedance of the protective earth return path is non-negligible, and includes the "stator frame–bogie–vehicle body–protective resistor–return busbar–grounding brushes–wheelset contact." Additionally, for railway vehicles operating at low speed, the rotor is grounded via the gearbox to earth potential, which forms a lower impedance path than the grounding of the stator frame.
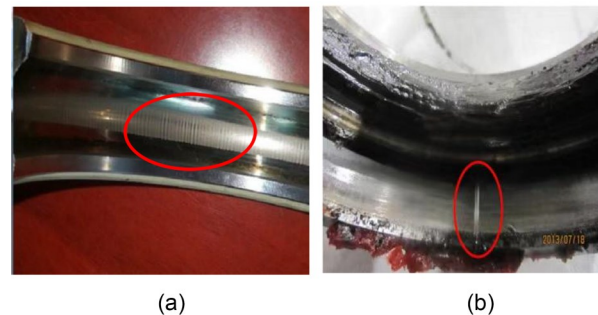

(a)   (b)

Fig. 4 Bearing failures in metro vehicles (a) and electric multiple units (EMU) trains (b)

In this paper, we provide a review of electrical bearing current phenomena in railway vehicles. In the following sections, the mechanisms that generate bearing currents, classified into four categories, are introduced first. Then, the established models for analyzing bearing currents are reviewed, including railway vehicle system configurations and the related impedance determination of the coupling path. In addition, the strategies frequently used in the industry for bearing protection are summarized, and a typical solution used to suppress electrical bearing failures in railway vehicles is described. Finally, a case study is presented to illustrate the research procedure for the systematic investigation of inverter-induced bearing currents in railway vehicles.

2 Analysis and modeling of bearing currents

2.1 Classification of bearing currents

The origin of the bearing current phenomena is the CM voltage v_{cm}, which is defined by the arithmetic mean of the line-to-ground voltages (Eq. (1)). Due to the discrete switching states in PWM, the sum of three output voltages is not equal to zero. The HF components of this voltage interact with the parasitic capacitances of the motor, exciting the inverter-induced bearing currents, which can be further classified into non-circulating and circulating bearing currents by their flow paths.

$$v_{cm} = \frac{v_{UG} + v_{VG} + v_{WG}}{3}, \qquad (1)$$

where v_{UG}, v_{VG}, and v_{WG} are the voltages of the three inverter phases U, V, and W to ground, respectively.

The non-circulating type of bearing currents includes the dv/dt, EDM, and rotor ground bearing currents. At elevated motor speed, the lubricating film of the bearing has insulating properties, and the bearing acts as a capacitor C_b. When the rotor is not grounded, the CM voltage generates bearing voltage v_b across the bearing due to the voltage divider of the motor parasitic capacitances. The ratio between v_b and v_{cm} is named the bearing voltage ratio (BVR), and can be calculated as follows:

$$\mathrm{BVR} = \frac{v_b}{v_{cm}} = \frac{C_{wr}}{C_{wr} + C_{rf} + 2C_b}. \qquad (2)$$

The dv/dt bearing currents can be capacitive or conductive (Bhattacharya et al., 1999). At each switching instant, the charge/discharge capacitive currents flow through the path of the "stator winding–rotor–bearing–stator frame," and their magnitudes are given by Eq. (3). However, at low motor speed, the lubrication film is bridged by metallic contact. In this case, the bearing is an ohmic resistance, and conductive currents are generated. In the literature, the effect of this kind of bearing current is neglected because of its much smaller amplitude (typically 5–200 mA) than other types of bearing currents (Muetze and Binder, 2007a).

$$i_{b,\,dv/dt} = C_b \cdot \frac{dv_b}{dt}, \qquad (3)$$

where $i_{b,\,dv/dt}$ is the capacitive or conductive bearing current.

EDM bearing currents occur when the threshold voltage of the lubricating film is surpassed by the bearing voltage v_b. According to Eq. (2), high CM voltages are more likely to result in EDM current pulses. These currents are a function of the bearing impedance (C_b, R_b) and the bearing voltage at the breakdown ($v_{b,th}$), and these parameters will be further affected by the bearing temperature, motor speed, and bearing load (Magdun et al., 2010a; Tischmacher and Gattermann, 2010). Furthermore, a controlled switch can be used to mimic the statistically distributed lubrication film breakdown process of EDM currents (Muetze, 2004; Muetze and Binder, 2007d). The peak value of EDM current impulse ($i_{b,\,EDM\_max}$) can be evaluated by Eq. (4) (Magdun et al., 2011). Typical peak amplitudes for EDM currents are 0.5–3.0 A.

$$i_{b,\,EDM\_max} = \frac{v_{b,th}}{R_b}. \qquad (4)$$

Rotor ground bearing currents arise when the rotor-to-ground impedance is lower than the stator-to-ground impedance (Muetze, 2004; Muetze and Binder, 2006). In this case, the bearing voltage is reconfigured, which results in considerable rotor ground bearing currents $i_{b,rg}$ flowing through "stator winding–stator frame–bearing–rotor–ground." $i_{b,rg}$ may reach considerable magnitudes (1–35 A) and is harmful to the bearings.

Unlike the non-circulating bearing currents, the generation of a circulating current is due to both inductive coupling and capacitive coupling. The steep edges of the HF CM voltage at the motor terminals couple with the parasitic capacitance C_{wf}, generating the HF CM current i_{cm} flowing through the stator core. This causes an alternating flux ϕ_{cir} encircling the shaft, and inducing a voltage v_{sh} along the motor shaft. If v_{sh} is capable of puncturing the bearing lubrication film, the HF bearing currents (0.5–20 A) circulate in the loop "stator frame–non drive end–shaft–drive end." This type of bearing current mirrors i_{cm} and flows in opposite directions in two bearings (Chen and Lipo, 1998; Muetze and Binder, 2007b).

Based on the above analysis, for large motors in railway vehicles, the rotor ground bearing currents and circulating bearing currents are major contributors to

inverter-induced bearing failures. According to experimental results (Muetze and Binder, 2006, 2007a), a proper thickness of insulation can reduce the HF circulating bearing currents to less than 40% of the values associated with non-insulated bearings. Therefore, the rotor ground bearing currents are the main cause of bearing electrical erosion in railway vehicles.

2.2 Modeling of non-circulating bearing currents

Chen ST et al. (1996) first proposed the equivalent lumped parameter circuit model of inverter-induced bearing currents. On the basis of the transmission line theory, an equivalent lumped parameter π-network is used for a simplified analysis of the parasitic coupling phenomenon. However, the model parameters need to be identified by matching simulation results with experimental measurements. For a more comprehensive understanding of the phenomena, Busse et al. (1997a, 1997b, 1997c, 1997d, 1997e) proposed the resistance-inductance-capacitance (RLC) equivalent circuit model. The model provides an efficient tool for the analysis of system parameters, such as the inverter output CM voltage, series and parallel impedance elements (Z_{series} and Z_{parallel}, e.g. long cables, CM chokes, transformers, and line reactors), the stator windings zero-sequence impedance (Z_0), and their influence on bearing currents. In addition, Muetze (2004) used a controllable switch to model the breakdown process of the lubrication film and investigated the inaccuracy of the measurable and real bearing currents. To discuss the effect caused by the presence of the

rotor grounding path, the bearing current model was extended by adding the frame-to-ground impedance Z_{fg} and rotor-to-ground impedance Z_{rg} (Guttowski et al., 2006; Liu et al., 2015a). Based on the above analysis, a model of non-circulating bearing currents is depicted in Fig. 5.
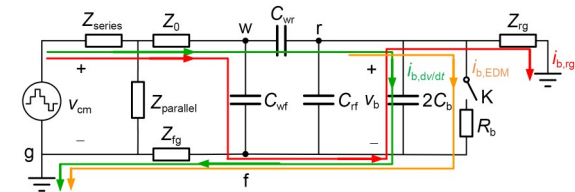

Fig. 5 Equivalent circuit model for non-circulating bearing currents

However, the system configurations for rail transportation are more complicated (Fig. 6) (Zhang, 2008; Yan et al., 2019). For metro vehicles, the positive supply rail of the inverter is connected to 1500 V DC, and the negative one is connected to the return bus bar. The bus bar is further grounded to the wheel with earth return devices, which provide return paths for both working earthing and protective earthing. The protective earthing connection for traction motors includes "motor frame–bogie chassis–vehicle body–protective resistor–bus bar." For EMU trains, the system is powered by 25 kV/50 Hz, and the supply voltage for the single-phase rectifier is lowered to 900 V with a step-down transformer. Unlike metro vehicles, the earth return devices are installed at the bogie chassis. Thus, the tractive current returns to the ground via "vehicle
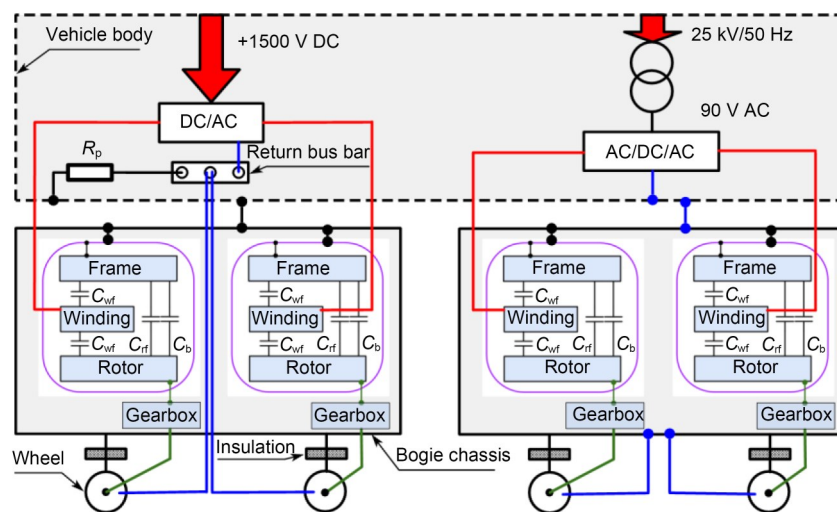

Fig. 6 System configurations for railway vehicles

body–bogie chassis–earth return devices," and the working earthing for traction motors is simplified to "motor frame–bogie chassis–earth return devices." In addition, for railway vehicles, the rotor is grounded with a low-impedance path consisting of "rotor–shaft coupling–gearbox–wheel." Therefore, the bearing currents have two coupling paths. The motor frame grounding impedance of metro vehicles is higher than that of EMU trains, which means metro vehicles are more prone to bearing electric erosion caused by rotor ground bearing currents.

2.3 Determination of coupling capacitances

For HF components of CM voltage less than 100 kHz, the coupling paths are simplified to be pure capacitive, including three equivalent parasitic capacitances and two bearing capacitances. Theoretical methods for calculating equivalent capacitances can be classified as analytical methods (Busse et al., 1997d; Muetze, 2004; Liu et al., 2014a; Wang et al., 2015) or finite element methods (FEMs) (Magdun et al., 2010b; Liu et al., 2014a, 2015b). A schematic of a stator slot segment is shown in Fig. 7, which illustrates the parameters used in an analytical method.
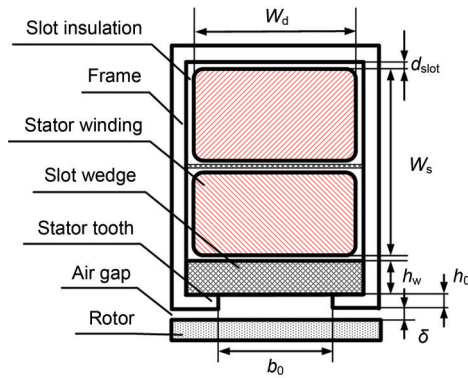

Fig. 7 Schematic of a stator slot segment used in an analytical method

Busse et al. (1997d) first introduced the analytical calculation of C_{wf}, which consists of N_s parallel capacitors. Each slot is modeled as a rectangular conductor, with length l_{Fe}, width W_d, and depth W_s. The dielectric material separates the stator winding and frame by d_{slot} with a relative permittivity of ε_{r1}. The effect of the winding irregular surface is considered by the factor F_c (Muetze, 2004), which is in the order of 0.8 to 1, and set as 1 in this paper, for simplicity. With these assumptions, C_{wf} is calculated as

$$C_{wf} = F_c N_s \varepsilon_{r1} \varepsilon_o \frac{(W_d + 2W_s) l_{Fe}}{d_{slot}}, \quad (5)$$

where the permittivity of the vacuum $\varepsilon_0 = 8.854 \times e^{-12}$ F/m. Additionally, Adabi et al. (2010) considered the stator windings-to-stator teeth equivalent capacitance, which makes the results more accurate.

The capacitance C_{rf1} is considered as that of a cylindrical air-insulated capacitor between the rotor surface and stator iron (Busse et al., 1997d). On this basis, the Carter coefficient k_c is introduced to account for the influence of the stator slot openings. Since the air gap length δ is much smaller than the outer diameter of the rotor d_{re}, the analytical expression of C_{rf1} is further simplified as (Muetze, 2004):

$$C_{rf1} = \varepsilon_0 l_{Fe} \frac{\pi d_{re}}{k_c \delta}, \quad (6)$$

$$k_c = \frac{B_{\delta max}}{B_{\delta av}}, \quad (7)$$

where $B_{\delta av}$ is the average magnetic field density in the air gap along the circumference, and $B_{\delta max}$ is the maximum magnetic field density in the air gap. Generally, k_c is slightly greater than 1, and is set to 1 in this paper, for simplicity.

The analytical calculation of stator winding-to-rotor capacitance C_{wr} was first proposed by Busse et al. (1997d). C_{wr} consists of N_s sets of parallel plate capacitors formed by the stator coils in slots and the rotor surface, with width W_d, length l_{Fe}, and a dielectric distance of δ. However, the method neglects the effect of the slot wedge and stator slot opening. Subsequently, C_{wr} is modeled as a series connection of the capacitance of the air gap δ and the slot opening h_0, and the capacitance of the slot wedge h_w and the slot insulation d_{slot} (Muetze, 2004), which can be calculated as

$$\begin{cases} C_{wr0} = \dfrac{N_s \varepsilon_0 b_0 l_{fe}}{\delta + h_0}, \\ C_{wr1} = \dfrac{N_s \varepsilon_{r1} \varepsilon_0 b_0 l_{fe}}{h_w + d_{slot}}, \\ C_{wr} = \dfrac{1}{\dfrac{1}{C_{wr0}} + \dfrac{1}{C_{wr1}}}, \end{cases} \quad (8)$$

where b_0 is the width of the stator tooth. For more accuracy, the capacitance formed by stator windings,

stator teeth, and rotor surface is considered (Adabi et al., 2010).

Magdun et al. (2010b) first presented the FEM calculation of motor capacitances. Based on the electric field energy calculation, the capacitances are calculated using a 2D solid conductor model. Although C_{rfl} is correctly calculated, the distribution of the stator windings in the slot and their end effects are not considered. To this end, the scattered line model along with the 3D FEM was introduced to increase the computational accuracy (Magdun et al., 2010b; Liu et al., 2014a, 2015b).

Busse et al. (1997d) first proposed the theoretical calculation of bearing capacitance, which comprises N_b parallel sphere capacitors formed by the ball element sphere (R_{ball}) and raceway sphere ($R_{ball}+b_g$):

$$C_b = \frac{4\pi N_b \varepsilon_o \varepsilon_{r2}}{\left(\dfrac{1}{R_{ball}} - \dfrac{1}{R_{ball}+b_g}\right)}, \tag{9}$$

where ε_{r2} is the relative permittivity of the lubrication film.

However, this methodology will result in significant inaccuracy of the capacitance value due to the inappropriate simplification of the sphere capacitor. Combined with elastic deformation and fluid mechanics analysis, the formulas of the grease film thickness h_{Hertz} and the Hertzian contact area S_{Hertz} are obtained, then the bearing capacitance C_{Hz} can be evaluated by Eq. (10) (Muetze, 2004). To improve the cxalculation accuracy, the electrical coupling between the ball elements and inner/outer ring is considered by C_{air} (Fig. 8) (Magdun and Binder, 2009; Liu et al., 2014b).

$$C_{Hz} = \varepsilon_{r2}\varepsilon_0 \frac{S_{Hertz}}{h_{Hertz}}. \tag{10}$$

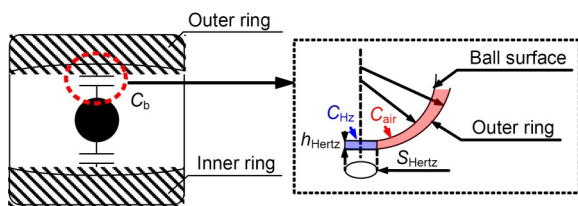Additionally, a novel approach to calculating the equivalent bearing capacitance was proposed by Liu

Fig. 8 Schematic of ball bearing model for capacitance calculation

et al. (2017). On the basis of the elastohydrodynamic lubrication analysis, h_{Hertz} can be determined. Thus, 3D bearing models can then be established in ANSYS Maxwell finite element analysis software and the capacitance can be obtained.

3 Techniques for suppressing bearing currents

The main purpose of investigating bearing current phenomena is to prolong the bearing life and achieve long-term reliability. Numerous strategies have been put forward to suppress bearing currents, and according to their functions, these methodologies can be categorized into two groups.

The first group includes inverter-side mitigation strategies that target the HF CM voltage caused by PWM inverters. The schematic diagram of a typical converter-motor system is shown in Fig. 2. The calculation of CM voltage can be written as Eq. (11), which includes two parts.

$$v_{cm} = \frac{v_{UO} + v_{VO} + v_{WO}}{3} + v_{OG} = \\ \frac{v_{UO} + v_{VO} + v_{WO}}{3} + \frac{v_{PG} + v_{NG}}{2} = v_{cm1} + v_{cm2}. \tag{11}$$

Under the assumption of $v_{OG}=0$, the case is simplified to a three-phase two-level inverter-motor system and the CM voltage levels include $\pm v_{dc}/6$ and $\pm v_{dc}/2$, forming a four-level staircase waveform. The analytical harmonic solution for v_{cm1} with double-edge naturally sampled PWM can be described as (Holmes and Lipo, 2003):

$$v_{cm1} = \frac{v_{dc}}{2} + \frac{2v_{dc}}{\pi}\left\{\sum_{m=2k-1}^{\infty} (-1)^{\frac{m-1}{2}} \frac{1}{m} J_0\left(m\frac{\pi}{2}M\right) \times \right.$$
$$\cos(m\omega_c t) + \sum_{m=2k-1}^{\infty}\sum_{n=6l}^{\infty} \frac{1}{m} J_n\left(m\frac{\pi}{2}M\right)\sin\left[(m+n)\frac{\pi}{2}\right] \times$$
$$\cos\left[(m\omega_c \pm n\omega_r)t\right] + \sum_{m=2k}^{\infty}\sum_{n=6l-3}^{\infty} \frac{1}{m} J_n\left(m\frac{\pi}{2}M\right) \times$$
$$\left. \sin\left[(m+n)\frac{\pi}{2}\right]\cos\left[(m\omega_c \pm n\omega_r)t\right]\right\}, \tag{12}$$

where M is the modulation index, ω_c is the carrier wave angular frequency, ω_r is the fundamental wave angular frequency, and J_n is the Bessel function of

order n. From Eq. (12), v_{cm1} consists of odd carrier harmonics and sideband harmonics with even combinations of $m \pm n$, while the fundamental component and even carrier harmonics are eliminated. For the second part v_{cm2}, v_{PG} and v_{NG} are determined by the conducting diodes of the input rectifier. The sum of the v_{PG} and v_{NG} oscillates with a frequency equal to three times the frequency of the source voltage (Tischmacher et al., 2015; Furtmann et al., 2016). The simulation waveforms of v_{cm}, v_{cm1}, and v_{cm2} and their respective fast Fourier transform (FFT) spectra are depicted in Fig. 9.

From the above analysis of v_{cm}, the most direct approach for bearing current mitigation techniques is to lower the switching frequency with limited control
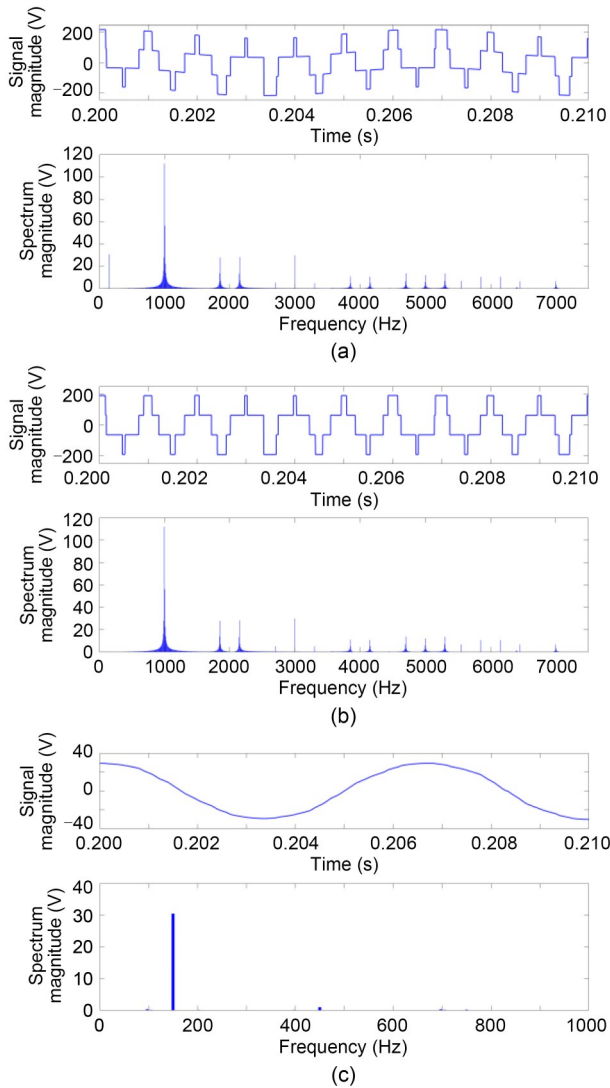

Fig. 9 Simulation waveforms of v_{cm} (a), v_{cm1} (b), and v_{cm2} (c) and their respective FFT spectra (sinusoidal pulse width modulation, f_c=1 kHz)

performance (Muetze and Binder, 2007d), which is not recommended. Filter techniques are used to reduce the HF CM voltage at the motor terminals, such that the bearing voltage is kept in check (Hyypio, 2005; Akagi and Tamura, 2006; Hedayati et al., 2013). Without additional hardware costs, the CM voltage is limited by advanced PWM control techniques (Un and Hava, 2009; Han et al., 2019). Compared with the conventional modulation techniques such as space vector PWM and discontinuous PWM, the peak amplitude of CM voltages generated by the active zero state PWM and near-state PWM is reduced from $\pm v_{dc}/2$ to $\pm v_{dc}/6$. On the other hand, the CM voltage can be naturally suppressed by multilevel inverters (Wang, 2000; Zhang et al., 2000). In addition, Muetze and Sullivan (2011) suppressed CM currents using magnetic rings that have an easy-to-install design and a simple structure. Experimental results show that these low-cost CM chokes can effectively reduce the circulating bearing currents and rotor ground bearing currents, while having little effect on the EDM bearing currents.

The second group consists of mitigation strategies in the motor. The most commonly used method is to break the HF bearing current loops with insulated/hybrid/full ceramic bearings (Muetze and Binder, 2007c; Plazenet et al., 2018). Insulated bearings are steel bearings with an insulating aluminum oxide layer deposited on the outer surface of the outer bearing ring. These bearings already have been used to suppress classical, circulating, and rotor ground bearing currents. For small motors that suffer from EDM bearing currents, hybrid bearings consisting of steel bearing rings and ceramic bearing rolls/balls are recommended. Although hybrid bearings can suppress all kinds of bearing currents completely, less expensive insulated bearings are more commonly used since they are sufficient to suppress the bearing currents for large machines (Muetze and Binder, 2006). Full ceramic bearings have inner/outer races and balls made of either silicon nitride, zirconium oxide, or silicon carbide. These are designed for applications operating in extreme special environments where conventional bearings are not suitable, such as vacuum environments and semiconductor manufacturing. Another typical approach is to use the shaft grounding mechanism to ensure a low potential on the motor shaft. In industry, many trouble-free AC motor applications are protected against bearing voltages by means of specially

designed brushes, which provide a low-impedance path to ground for the harmful bearing currents. Based on similar principles, an alternative brush concept with less maintenance than traditional grounding brushes is emerging in the industry (Muetze and Oh, 2008a, 2008b, 2010). Making use of conductive microfibers, this kind of brush has ultralow friction and is very robust toward contamination. Besides, it is particularly suitable for use with EDM and circulating bearing currents. Although being the opposite of insulating methods, greases with enhanced conductivity are effective in preventing fluting (Suzumura, 2016). However, there is still a lack of industrial lubricants with superior conductivities and outstanding lubricities. Furthermore, Busse et al. (1997d) proposed a modified induction motor by mounting a Faraday shield in the air gap between the stator and rotor. Experimental results prove that the electrostatic shielded induction motor solves the inverter-induced bearing voltage with increased eddy current loss. Likewise, grounded slot wedges or electrodes can be constructed in the stator slots to suppress EDM bearing currents using the electrostatic shield principle (Ferreira et al., 2012; Bai et al., 2015; Vostrov et al., 2021). In addition, recent studies addressing the problem by modifying the design of the electric machine provide a different perspective (Yea and Han, 2020; Berhausen and Jarek, 2022).

For railway vehicles, the problems of bearing currents are commonly solved by the bearing insulation and shaft grounding mechanism because of their technological maturity and ease of implementation. In addition, inspired by the mechanism of generation of rotor ground bearing currents, researchers suggest this kind of bearing current can be limited by optimizing the grounding configuration (Liu et al., 2015a; Yan et al., 2019; Chen, 2021; Luo, 2021). Taking metro vehicles as an example, the commonly used topology is shown in Fig. 10, where the vehicle body is connected to the return bus bar with a protective resistor. Then, the bus bar is grounded to wheels via the earth return devices. Accordingly, the overall protective earthing loop is so long that the equivalent grounding impedance at the motor frame has an order of magnitude similar to that at the motor shaft, which means considerable HF grounding currents will flow across the bearing. To reduce the cable length between the vehicle body and earthing device, a protective resistor

is installed at each bogie chassis for each car body, which is referred to as the "double-resistor scheme" (Fig. 10). In this case, the vehicle body is directly grounded with the protective resistor above the bogie chassis, and the grounding impedance Z_{fg} is significantly decreased. Consequently, HF motor grounding currents are more likely to flow back to earth through Z_{fg} compared with Z_{rg}, which suppresses the bearing currents.
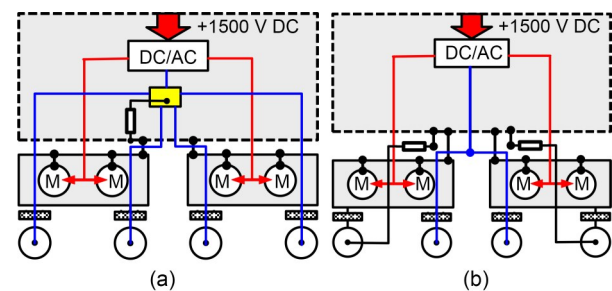
Fig. 10 Grounding configuration before (a) and after (b) optimization

4 Case example

Here, we describe a case example to illustrate the research procedure for the systematic investigation of inverter-induced bearing currents in railway vehicles. It involves an inverter-driven 190-kW four-pole squirrel cage induction motor with insulated bearings, used in a metro project.

First, the mechanism of generation of the bearing currents is identified. For metro vehicles operating at low speed, a lubrication film in the gearbox is not formed. The rotor is grounded to the axle via a non-insulated coupling and a short-circuited gearbox. In this case, rotor ground bearing currents are the main cause of bearing electric erosion. At elevated running speed, a lubrication film with small capacitance on the gear meshing surface is formed, which blocks the rotor grounding path. A four-level staircase bearing voltage waveform along with EDM currents is generated. For a 190-kW motor, such EDM bearing currents are not likely to cause much bearing damage, but the endangerment of bearings due to rotor ground bearing currents at low speed should be investigated.

Next, the equivalent circuit model of the metro traction system is proposed (Fig. 11). The related parameters are explained in Table 1. The CM voltage

Fig. 11 Equivalent circuit model of metro traction system

Table 1 Explanation of parameters in the equivalent circuit model

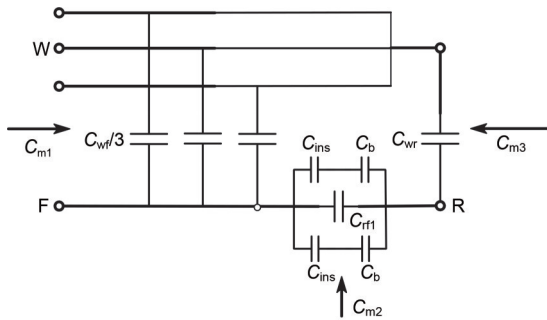| Parameter	Explanation
C	Inverter bulk capacitor
C_{emi}	Electromagnetic interference capacitor
L	Inverter input inductance
L_0	Stator–winding leakage inductance
L_{cb}	Bogie-to-body inductance
L_p	Grounding protection stray inductance
R_p	Grounding protection resistor
L_2	Bus bar–wheel cable inductance
R_2	Bus bar–wheel resistance
L_1	Inverter–bus bar inductance
C_t	Gear meshing surface stray capacitance
L_t	Shaft coupling stray inductance

generated by the traction inverter couples with the motor parasitic capacitances and system earthing impedances, forming a current flowing through the bearing.

Then, related parameters are determined to predict the bearing voltage in such a system configuration. Through field research, the switching frequency of the traction inverter is in the range of 400 to 1500 Hz, and is set to 1000 Hz in the simulation. The electromagnetic interference (EMI) capacitor is equal to 1 μF and the cable inductance L_2 is set as 0.5 μH. L_0 can be extracted by the port impedance test results measured by the impedance analyzer (Magdun and Binder, 2014; Zhao et al., 2021), which is 48.1 μH.

The coupling capacitances in the motors are analytically calculated with some simplification based on Eqs. (5)–(8). For C_{wf}, we assume the slots are to be filled with stator windings and slot insulation, and the surface of the windings is regular ($F_c=1$). C_{wr} is formed as a series connection of capacitors, including the slot insulation, slot wedge, and air. For simplification, the permittivity of slot insulation is set as the same as that

of the slot wedge. In this way, the analytical value of C_{wr} can be calculated using Eq. (8). Note that, for motors with insulated bearings, the capacitance of the insulating layer C_{ins} should be included in the calculation of C_{rf} in the static state. In addition, the 3D model of the structure of stator and rotor is established (Fig. 12). The theoretical results are listed in Table 2 (Zhou et al., 2022).

Fig. 12 3D model of the structure of the stator and rotor

Table 2 Calculated motor equivalent capacitances

Item	C_{wf} (pF)	C_{wr} (pF)	C_{rf} (pF)
Analytical	17500	227	13650
3D ANSYS	17670	258	14100
Measured	16580	261	14401

In practice, the motor capacitances are measured using the method proposed by Liu et al. (2014a) (Fig. 13). For insulated motors, the measurement comprises the following steps: (1) keep the motor still; (2) use the inductance-capacitance-resistance (LCR) meter and three different configurations to derive C_{m1}, C_{m2}, and C_{m3}; (3) calculate C_{wf}, C_{wr}, and C_{rf} according to Eq. (13). The experimental results are listed in Table 2.

$$
\begin{aligned}
C_{m1} &= C_{wf} + \frac{C_{wr}C_{rf}}{C_{wr}+C_{rf}}, \\
C_{m2} &= C_{rf} + \frac{C_{wr}C_{wf}}{C_{wr}+C_{wf}}, \\
C_{m3} &= C_{wr} + \frac{C_{wf}C_{rf}}{C_{wf}+C_{rf}}.
\end{aligned}
\tag{13}
$$

Compared with the measured values of motor capacitances, the analytical result of C_{wf} is larger due to the assumption that the slots are full, which overestimates W_s in Eq. (5), while C_{wr} is smaller due to neglecting the effect of stator winding ends. The latter

Fig. 13 Diagram of capacitance measurement

problem is dealt with by the 3D ANSYS, and the calculated capacitance agrees well with the measured value. According to Muetze (2004) and Liu et al. (2017), the analytical result of bearing capacitance is 152 pF and the measured value is 171 pF. In comparison, the analytical result is smaller because S_{Hertz} is smaller than the actual area, and the electrical coupling air capacitance C_{air} is neglected.

To verify the correctness of the proposed equivalent circuit for the prediction of the bearing voltages in a metro vehicle traction system, simulations have been done in the MATLAB/Simulink environment and compared with the measured waveform of a metro project (Fig. 14). The peak bearing voltage is beyond 100 V in the starting and braking stages, and the staircase amplitude is much smaller at elevated speed. The four-level staircase waveform is not apparent for low-voltage utilization, and a reversed bearing voltage is observed due to the film discharge and switching state change. At low speed, the overlap of transient response makes the bearing voltage peak amplitude variable. The simulation waveforms of bearing voltage are shown in Fig. 15. Neglecting the film discharges, the staircase waveform is consistent with the experimental result. However, the voltage at low speed is not well predicted because the rising time of insulated gate bipolar transistors and the accuracy of parasitic parameters have great impacts on its waveform. With the equivalent circuit, the mechanism of generation and waveform characteristics of the bearing voltage are revealed.

Finally, mitigation techniques such as shaft grounding rings and grounding configuration optimization were applied to the metro projects to validate their effectiveness. With the use of the shaft grounding ring, the motor frame and shaft are short-circuited, and the bearing capacitance is isolated. The bearing voltage is significantly suppressed to 15 V (Fig. 16). However,
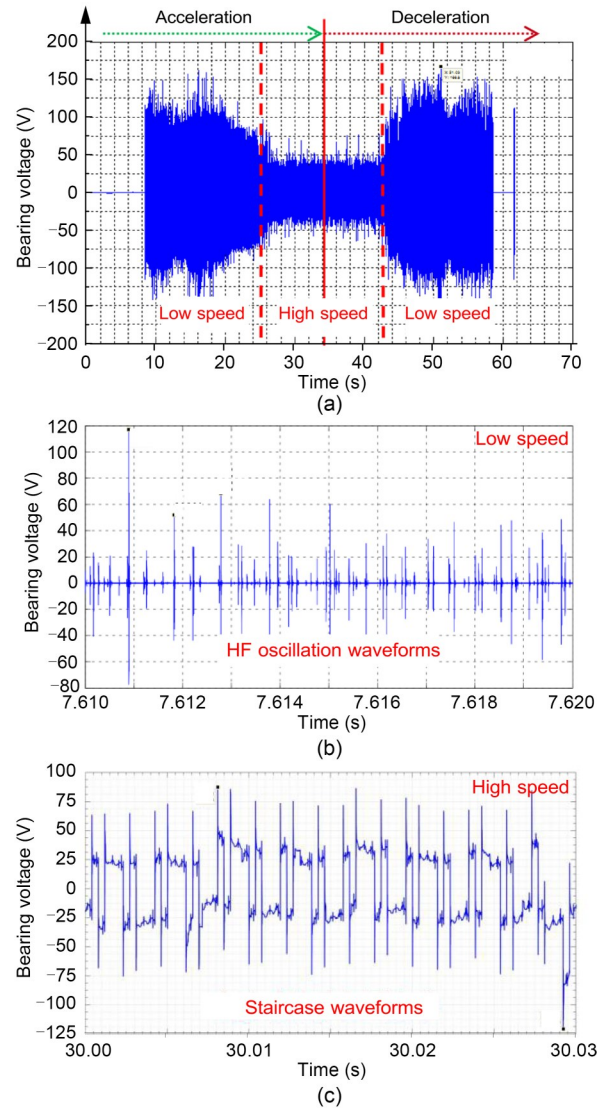

Fig. 14 Measured bearing voltage waveforms of a metro project with a single-resistor scheme: (a) overall waveform; (b) low-speed waveform; (c) high-speed waveform

the introduction of grounding rings may cause reflux through the vehicle body and gear meshing surface, which further leads to electromagnetic interference and gearbox damage. In addition, the service life and maintenance requirements are yet to be determined.

With improved grounding configurations, the value of equivalent grounding inductance L_2 is decreased, and more HF currents will flow through this path rather than across the bearing. Fig. 17 shows the test results using the double-resistor scheme for a domestic metro project. Compared with Fig. 14, the use of the double-resistor scheme appears to effectively reduce the bearing voltage.
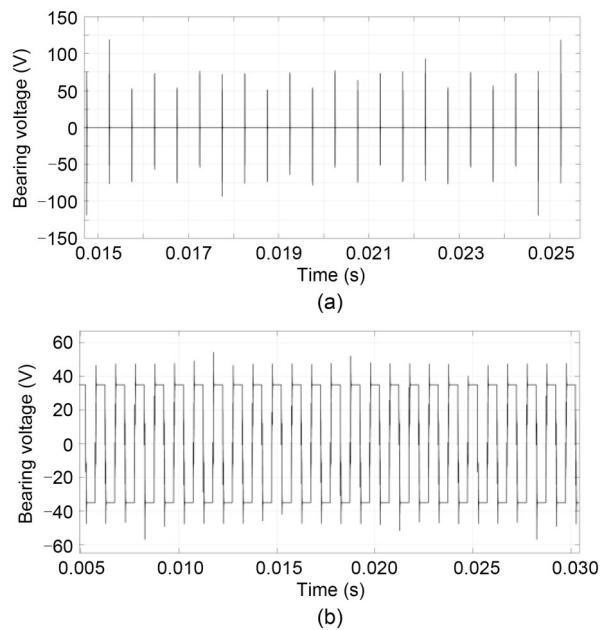
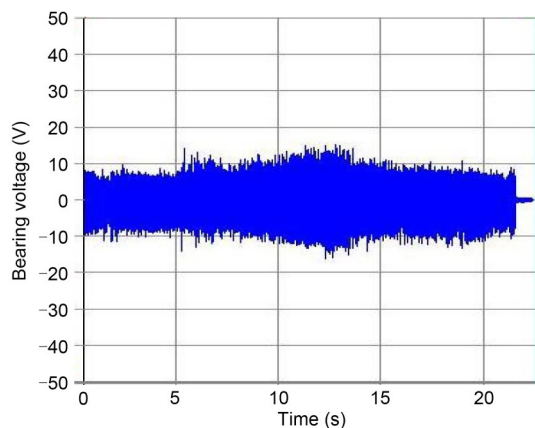**Fig. 15 Simulated bearing voltage waveform: (a) low speed; (b) high speed**

Fig. 16 Bearing voltage waveform with the use of shaft grounding rings
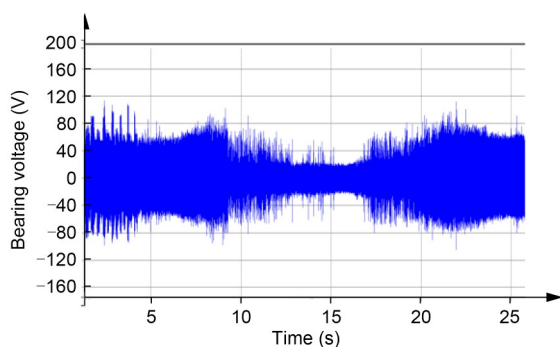

Fig. 17 Measured bearing voltage waveform of a metro project with the double-resistor scheme

5 Conclusions

The premature electrical failure of bearings has become a critical issue that has for decades restricted the lifetime of electric motor-based traction systems. In this study, an overview of electrical bearing failures in rail transportation has been presented. Related facets such as CM voltages, bearing electrical failure modes, generation and composition of bearing voltages and currents, modeling of bearing currents, and determination of coupling capacitances have been discussed to obtain a comprehensive and systematic perspective on the phenomena. On this basis, feasible ways to solve the problem are summarized, and a case study is presented to illustrate the research procedure recommended for the systematic investigation of inverter-induced bearing currents in rail transportation.

Despite the significant progress made in this area, further study is required in the following pertinent directions:

(1) A generalized prediction model for bearing currents. In this review, four typical bearing current modes are analyzed in simplified inverter-motor systems. However, the overall electrical system topology in practical applications is not consistent. For instance, the direct grounding of the motor frame and inverter is not achievable in metro vehicles, which complicates the composition of bearing currents. In these complex motor systems, more research is needed to predict the bearing currents quantitatively.

(2) Additional low-cost industrial bearing protection techniques. In Section 3, a summary of numerous bearing current mitigation techniques has been presented. Given their cost and reliability, it is still challenging to adopt these techniques for industrial use. Recent developments in lubrication materials with new electrical properties offer a broader perspective for possible solutions to bearing currents.

Acknowledgments

Author contributions

Yao LI conducted the literature survey and wrote the first draft of the manuscript. Yongjian ZHI, Zifan GAO, Jien MA, and Jian ZHANG assisted with the literature survey and

processed the experimental data. Lin QIU and Youtong FANG put forward the original idea of the proposed framework and supervised the research activities.

Conflict of interest

Yao LI, Lin QIU, Yongjian ZHI, Zifan GAO, Jien MA, Jian ZHANG, and Youtong FANG declare that they have no conflict of interest.

References

ABB, 2021. Rogowski Coil Current Sensors for Arc Flash Detection. ABB Review.
https://new.abb.com/news/detail/78554/rogo-wski-coil-current-sensors-for-arc-flash-detection

Adabi J, Zare F, Ghosh A, et al., 2010. Calculations of capacitive couplings in induction generators to analyse shaft voltage. *IET Power Electronics*, 3(3):379-390.
https://doi.org/10.1049/iet-pel.2008.0332

AEGIS, 2007. Shaft Grounding Rings for Low Voltage Motors.
https://www.est-aegis.com/product/sgr/

AEGIS, 2018. Bearing Protection Handbook: Best Practices for Bearing Protection in New and Repaired Motors, Testing In-Service Motors, and Inspecting Damaged Motor Bearings.
https://www.morganadvancedmaterials.com/media/7645/aegis-bearing-protection.pdf

Akagi H, Tamura S, 2006. A passive EMI filter for eliminating both bearing current and ground leakage current from an inverter-driven motor. *IEEE Transactions on Power Electronics*, 21(5):1459-1469.
https://doi.org/10.1109/TPEL.2006.880239

Alger PL, Samson HW, 1924. Shaft currents in electric machines. *Transactions of the American Institute of Electrical Engineers*, XLIII:235-245.
https://doi.org/10.1109/T-AIEE.1924.5060981

Ammann C, Reichert K, Joho R, et al., 1988. Shaft voltages in generators with static excitation systems-problems and solution. *IEEE Transactions on Energy Conversion*, 3(2):409-419.
https://doi.org/10.1109/60.4749

Bai BD, Wang Y, Wang XC, 2015. Suppression for discharging bearing current in variable-frequency motors based on electromagnetic shielding slot wedge. *IEEE Transactions on Magnetics*, 51(11):8109404.
https://doi.org/10.1109/TMAG.2015.2439961

Berhausen S, Jarek T, 2022. Analysis of impact of design solutions of an electric machine with permanent magnets for bearing voltages with inverter power supply. *Energies*, 15(12):4475.
https://doi.org/10.3390/en15124475

Bhattacharya S, Resta L, Divan DM, et al., 1999. Experimental comparison of motor bearing currents with PWM hard- and soft-switched voltage-source inverters. *IEEE Transactions on Power Electronics*, 14(3):552-562.
https://doi.org/10.1109/63.761699

Bonnett AH, Yung C, 2006. A construction, performance and reliability comparison for pre-EPAct, EPAct and premium-efficient motors. Record of Conference Papers–IEEE Industry Applications Society 53rd Annual Petroleum and Chemical Industry Conference.
https://doi.org/10.1109/PCICON.2006.359691

Boyanton HE, Hodges G, 2002. Bearing fluting [motors]. *IEEE Industry Applications Magazine*, 8(5):53-57.
https://doi.org/10.1109/MIA.2002.1028391

Boyd J, Kaufman HN, 1958. The causes and control of electrical currents in bearings. *Lubrication Engineering*, 2(6):28-35.

Buckley GW, Corkins RJ, Stephens RN, 1988. The importance of grounding brushes to the safe operation of large turbine generators. *IEEE Transactions on Energy Conversion*, 3(3):607-612.
https://doi.org/10.1109/60.8075

Busse DF, Erdman JM, Kerkman RJ, et al., 1997a. Bearing currents and their relationship to PWM drives. *IEEE Transactions on Power Electronics*, 12(2):243-252.
https://doi.org/10.1109/63.558735

Busse DF, Erdman JM, Kerkman RJ, et al., 1997b. Characteristics of shaft voltage and bearing currents. *IEEE Industry Applications Magazine*, 3(6):21-32.
https://doi.org/10.1109/2943.628116

Busse DF, Erdman JM, Kerkman RJ, et al., 1997c. The effects of PWM voltage source inverters on the mechanical performance of rolling bearings. *IEEE Transactions on Industry Applications*, 33(2):567-576.
https://doi.org/10.1109/28.568024

Busse DF, Erdman JM, Kerkman RJ, et al., 1997d. System electrical parameters and their effects on bearing currents. *IEEE Transactions on Industry Applications*, 33(2):577-584.
https://doi.org/10.1109/28.568025

Busse DF, Erdman JM, Kerkman RJ, et al., 1997e. An evaluation of the electrostatic shielded induction motor: a solution for rotor shaft voltage buildup and bearing current. *IEEE Transactions on Industry Applications*, 33(6):1563-1570.
https://doi.org/10.1109/28.649969

Chen SM, Lipo TA, Fitzgerald D, 1996. Source of induction motor bearing currents caused by PWM inverters. *IEEE Transactions on Energy Conversion*, 11(1):25-32.
https://doi.org/10.1109/60.486572

Chen ST, Lipo TA, 1998. Circulating type motor bearing current in inverter drives. *IEEE Industry Applications Magazine*, 4(1):32-38.
https://doi.org/10.1109/2943.644884

Chen ST, Lipo TA, Fitzgerald D, 1996. Modeling of motor bearing currents in PWM inverter drives. *IEEE Transactions on Industry Applications*, 32(6):1365-1370.
https://doi.org/10.1109/28.556640

Chen ZW, 2021. Comparative Study of Grounding Reflux Schemes for Metro Vehicles. MS Thesis, Beijing Jiaotong University, Beijing, China (in Chinese).

Cheng ZL, Zhou WH, Ding Z, et al., 2020. Estimation of spatiotemporal response of rooted soil using a machine learning approach. *Journal of Zhejiang University-SCIENCE A (Applied Physics & Engineering)*, 21(6):462-477.

https://doi.org/10.1631/jzus.A1900555

Costello MJ, 1993. Shaft voltages and rotating machinery. *IEEE Transactions on Industry Applications*, 29(2):419-426. https://doi.org/10.1109/28.216553

Ferreira FJTE, Cistelecan MV, De Almeida AT, 2012. Evaluation of slot-embedded partial electrostatic shield for high-frequency bearing current mitigation in inverter-fed induction motors. *IEEE Transactions on Energy Conversion*, 27(2):382-390. https://doi.org/10.1109/TEC.2012.2187452

Fleishmann L, 1910. Currents in bearings and shafts. *Elecktrische Kraftbetriebe and Bahnen*, 11(8):11-17 (in German).

Furtmann A, Tischmacher H, Poll G, 2016. Extended HF equivalent model of a drive train. XXII International Conference on Electrical Machines, p.2244-2250. https://doi.org/10.1109/ICELMACH.2016.7732834

Guttowski S, Weber S, Schinkel M, et al., 2006. Troubleshooting and fixing of inverter driven induction motor bearing currents in existing plants of large size–an evaluation of possible mitigation techniques in practical applications. Twenty-First Annual IEEE Applied Power Electronics Conference and Exposition, p.6. https://doi.org/10.1109/APEC.2006.1620544

Han Y, Lu HF, Li YD, et al., 2019. Analysis and suppression of shaft voltage in SiC-based inverter for electric vehicle applications. *IEEE Transactions on Power Electronics*, 34(7):6276-6285. https://doi.org/10.1109/TPEL.2018.2873079

Hedayati MH, Acharya AB, John V, 2013. Common-mode filter design for PWM rectifier-based motor drives. *IEEE Transactions on Power Electronics*, 28(11):5364-5371. https://doi.org/10.1109/TPEL.2013.2238254

Holmes DG, Lipo TA, 2003. Pulse Width Modulation for Power Converters: Principles and Practice. John Wiley & Sons, Inc., Hoboken, USA.

Hyypio D, 2005. Mitigation of bearing electro-erosion of inverter-fed motors through passive common-mode voltage suppression. *IEEE Transactions on Industry Applications*, 41(2):576-583. https://doi.org/10.1109/TIA.2005.844373

IEC (International Electrotechnical Commission), 2014. Rotating Electrical Machines—Part 25: AC Electrical Machines Used in Power Drive Systems—Application Guide, IEC TS 60034-25. IEC.

IEEE (Institute of Electrical and Electronics Engineers), 1997. IEEE Standard Test Procedure for Polyphase Induction Motors and Generators, IEEE Standard 112-1996. IEEE.

Liu RF, Chen JY, Ma XP, et al., 2014a. Calculation and measurement of coupling capacitances in AC motors based on bearing currents problem induced by PWM inverters. *Transactions of China Electrotechnical Society*, 29(1): 60-67 (in Chinese). https://doi.org/10.19595/j.cnki.1000-6753.tces.2014.01.009

Liu RF, Lou ZF, Ma XP, et al., 2014b. Modeling of bearing capacitance and resistance in motor bearing current problem. *Proceedings of the CSEE*, 34(15): 2430-2437 (in Chinese).

https://doi.org/10.13334/j.0258-8013.pcsee.2014.15.013

Liu RF, Sang BQ, Cao JC, 2015a. Investigation on the influence of motors grounding states on bearing voltage in inverter drive system. *Proceedings of the CSEE*, 35(S1):177-183 (in Chinese). https://doi.org/10.13334/j.0258-8013.pcsee.2015.S.024

Liu RF, Li JF, Sang BQ, et al., 2015b. Modeling of coupled capacitances and bearing voltage in induction motors fed by inverters based on numerical calculation of electromagnetic field. *Transactions of China Electrotechnical Society*, 30(14):161-169 (in Chinese). https://doi.org/10.3969/j.issn.1000-6753.2015.14.022

Liu RF, Sang BQ, Li WL, 2017. Calculations and measurements of bearing capacitance in AC motor bearings. *Proceedings of the CSEE*, 37(10):2986-2993 (in Chinese). https://doi.org/10.13334/j.0258-8013.pcsee.160610

Luo ZX, 2021. Research on traction motor bearing electric erosion of metro vehicle and its improvement measures. *Electric Drive for Locomotives*, (2):37-41 (in Chinese). https://doi.org/10.13890/j.issn.1000-128x.2021.02.007

Magdun O, Binder A, 2009. Calculation of roller and ball bearing capacitances and prediction of EDM currents. The 35th Annual Conference of IEEE Industrial Electronics, p.1051-1056. https://doi.org/10.1109/IECON.2009.5414669

Magdun O, Binder A, 2014. High-frequency induction machine modeling for common mode current and bearing voltage calculation. *IEEE Transactions on Industry Applications*, 50(3):1780-1790. https://doi.org/10.1109/TIA.2013.2284301

Magdun O, Gemeinder Y, Binder A, 2010a. Investigation of influence of bearing load and bearing temperature on EDM bearing currents. IEEE Energy Conversion Congress and Exposition, p.2733-2738. https://doi.org/10.1109/ECCE.2010.5618061

Magdun O, Gemeinder Y, Binder A, 2010b. Prevention of harmful EDM currents in inverter-fed AC machines by use of electrostatic shields in the stator winding overhang. The 36th Annual Conference on IEEE Industrial Electronics Society, p.962-967. https://doi.org/10.1109/IECON.2010.5675498

Magdun O, Gemeinder Y, Binder A, et al., 2011. Calculation of bearing and common-mode voltages for the prediction of bearing failures caused by EDM currents. The 8th IEEE Symposium on Diagnostics for Electrical Machines, Power Electronics & Drives, p.462-467. https://doi.org/10.1109/DEMPED.2011.6063664

Muetze A, 2004. Bearing Currents in Inverter-Fed AC-Motors. PhD Thesis, Technische Universität Darmstadt, Darmstadt, Germany.

Muetze A, Binder A, 2006. Don't lose your bearings. *IEEE Industry Applications Magazine*, 12(4):22-31. https://doi.org/10.1109/MIA.2006.1678327

Muetze A, Binder A, 2007a. Calculation of circulating bearing currents in machines of inverter-based drive systems. *IEEE Transactions on Industrial Electronics*, 54(2):932-938. https://doi.org/10.1109/TIE.2007.892001

Muetze A, Binder A, 2007b. Calculation of motor capacitances for prediction of the voltage across the bearings in machines of inverter-based drive systems. *IEEE Transactions on Industry Applications*, 43(3):665-672. https://doi.org/10.1109/TIA.2007.895734

Muetze A, Binder A, 2007c. Practical rules for assessment of inverter-induced bearing currents in inverter-fed AC motors up to 500 kW. *IEEE Transactions on Industrial Electronics*, 54(3):1614-1622. https://doi.org/10.1109/TIE.2007.894698

Muetze A, Binder A, 2007d. Techniques for measurement of parameters related to inverter-induced bearing currents. *IEEE Transactions on Industry Applications*, 43(5):1274-1283. https://doi.org/10.1109/TIA.2007.904413

Muetze A, Oh HW, 2008a. Application of static charge dissipation to mitigate electric discharge bearing currents. *IEEE Transactions on Industry Applications*, 44(1):135-143. https://doi.org/10.1109/TIA.2007.912758

Muetze A, Oh HW, 2008b. Design aspects of conductive microfiber rings for shaft-grounding purposes. *IEEE Transactions on Industry Applications*, 44(6):1749-1757. https://doi.org/10.1109/TIA.2008.2006421

Muetze A, Oh HW, 2010. Current-carrying characteristics of conductive microfiber electrical contact for high frequencies and current amplitudes: theory and applications. *IEEE Transactions on Power Electronics*, 25(8):2082-2092. https://doi.org/10.1109/TPEL.2010.2046499

Muetze A, Sullivan CR, 2011. Simplified design of common-mode chokes for reduction of motor ground currents in inverter drives. *IEEE Transactions on Industry Applications*, 47(6):2570-2577. https://doi.org/10.1109/TIA.2011.2170101

Plazenet T, Boileau T, 2021. Overview of bearing white etching cracks due to electrical currents. IEEE 13th International Symposium on Diagnostics for Electrical Machines, Power Electronics and Drives, p.440-446. https://doi.org/10.1109/SDEMPED51010.2021.9605561

Plazenet T, Boileau T, Caironi C, et al., 2018. A comprehensive study on shaft voltages and bearing currents in rotating machines. *IEEE Transactions on Industry Applications*, 54(4):3749-3759. https://doi.org/10.1109/TIA.2018.2818663

Punga F, Hess W, 1907. Bearing currents. *Elektrotechnik und Maschinenbau*, 25(8):615-618 (in German).

Raymond OKJ, 1999. An Investigation of Shaft Current in a Large Sleeve Bearing Induction Machine. PhD Thesis, McMaster University, Ontario, Canada.

Shamsirband S, Khansari NM, 2021. Micro-mechanical damage diagnosis methodologies based on machine learning and deep learning models. *Journal of Zhejiang University-SCIENCE A (Applied Physics & Engineering)*, 22(8):585-608. https://doi.org/10.1631/jzus.A2000408

SKF, 2014. Electrical Discharge Detector Pen. SKF. https://www.skf.com/group/products/condition-monitoring-systems/basic-condition-monitoring-products/electrical-discharge-current-measurement

SKF, 2019. SKF @ptitude Analyst. https://www.skf.com/binaries/pub12/Images/0901d19680 59796b-PUB-CM-P8-10299-12-EN-SKF-Aptitude-Analyst-brochure_tcm_12-582180.pdf

SKF, 2022. The Future of Bearing Failure Analysis is Here. https://evolution. skf. com/en/the-future-of-bearing-failure-analysis-is-here/

Sunahara K, Ishida Y, Yamashita S, et al., 2011. Preliminary measurements of electrical micropitting in grease-lubricated point contacts. *Tribology Transactions*, 54(5):730-735. https://doi.org/10.1080/10402004.2011.597543

Suzumura J, 2016. Prevention of electrical pitting on rolling bearings by electrically conductive grease. *Quarterly Report of RTRI*, 57(1):42-47. https://doi.org/10.2219/rtriqr.57.1_42

Tischmacher H, Gattermann S, 2010. Bearing currents in converter operation. The XIX International Conference on Electrical Machines, p.1-8. https://doi.org/10.1109/ICELMACH.2010.5608126

Tischmacher H, Gattermann S, 2012a. Investigations on bearing currents in converter-fed electrical motors. The XXth International Conference on Electrical Machines, p.1764-1770. https://doi.org/10.1109/ICElMach.2012.6350120

Tischmacher H, Gattermann S, 2012b. Multiple signature analysis for the detection of bearing currents and the assessment of the resulting bearing wear. International Symposium on Power Electronics Power Electronics, Electrical Drives, Automation and Motion, p.1354-1359. https://doi.org/10.1109/SPEEDAM.2012.6264380

Tischmacher H, Tsoumas IP, Furtmann A, 2015. Extended probability model for discharge activities in the drive train of converter-fed electric motors. The 17th European Conference on Power Electronics and Applications, p.1-10. https://doi.org/10.1109/EPE.2015.7309392

Un E, Hava AM, 2009. A near-state PWM method with reduced switching losses and reduced common-mode voltage for three-phase voltage source inverters. *IEEE Transactions on Industry Applications*, 45(2):782-793. https://doi.org/10.1109/TIA.2009.2013580

Vostrov K, Pyrhönen J, Lindh P, et al., 2021. Mitigation of inverter-induced noncirculating bearing currents by introducing grounded electrodes into stator slot openings. *IEEE Transactions on Industrial Electronics*, 68(12):11752-11760. https://doi.org/10.1109/TIE.2020.3045695

Wang F, 2000. Motor shaft voltages and bearing currents and their reduction in multilevel medium-voltage PWM voltage-source-inverter drive applications. *IEEE Transactions on Industry Applications*, 36(5):1336-1341. https://doi.org/10.1109/28.871282

Wang Y, Bai BD, Liu WF, et al., 2015. Hertz bearing current density calculation of variable frequency driven motors by frequency domain parasitic capacitance method. *Transactions of China Electrotechnical Society*, 30(2):189-195 (in Chinese). https://doi.org/10.19595/j.cnki.1000-6753.tces.2015.02.025

Yan GL, Zhi YJ, Chen X, et al., 2019. Research on mechanism and suppression technique of metro vehicles traction motor bearing electrocorrosion. *Electric Drive for Locomotives*, (4):102-106 (in Chinese).
https://doi.org/10.13890/j.issn.1000-128x.2019.04.113

Yea M, Han KJ, 2020. Modified slot opening for reducing shaft-to-frame voltage of AC motors. *Energies*, 13(3):760.
https://doi.org/10.3390/en13030760

Zhang DM, Zhang JZ, Huang HW, et al., 2020. Machine learning-based prediction of soil compression modulus with application of 1D settlement. *Journal of Zhejiang University-SCIENCE A (Applied Physics & Engineering)*, 21(6):430-444.
https://doi.org/10.1631/jzus.A1900515

Zhang HR, von Jouanne A, Dai SA, et al., 2000. Multilevel inverter modulation schemes to eliminate common-mode voltages. *IEEE Transactions on Industry Applications*, 36(6):1645-1653.
https://doi.org/10.1109/28.887217

Zhang PJ, Du Y, Habetler TG, et al., 2011. A survey of condition monitoring and protection methods for medium-voltage induction motors. *IEEE Transactions on Industry Applications*, 47(1):34-46.
https://doi.org/10.1109/TIA.2010.2090839

Zhang SG, 2008. CRH1 EMU. China Railway Publishing House, Beijing, China, p.134-166 (in Chinese).

Zhao QC, Yang EL, Liu RF, et al., 2021. Modeling of high frequency bearing currents of induction motors powered by frequency converters. *Proceedings of the CSEE*, 41(23):8139-8147 (in Chinese).
https://doi.org/10.13334/j.0258-8013.pcsee.210810

Zhao SF, Huang XY, Fang YT, et al., 2020. DC-link-fluctuation-resistant predictive torque control for railway traction permanent magnet synchronous motor in the six-step operation. *IEEE Transactions on Power Electronics*, 35(10):10982-10993.
https://doi.org/10.1109/TPEL.2020.2975497

Zhou LM, Huai XJ, Shen Z, et al., 2022. Common mode equivalent circuit modeling and parameter testing of traction motor. *Electric Locomotives & Mass Transit Vehicles*, 45(1):30-34.
https://doi.org/10.16212/j.cnki.1672-1187.2022.01.007